



OPEN

# Solution-processed small-molecule solar cells: breaking the 10% power conversion efficiency

SUBJECT AREAS:

SOLAR CELLS

ELECTRONIC MATERIALS

ELECTRONIC DEVICES

SOLAR ENERGY AND  
PHOTOVOLTAIC  
TECHNOLOGYYongsheng Liu<sup>1,2\*</sup>, Chun-Chao Chen<sup>1\*</sup>, Ziruo Hong<sup>1</sup>, Jing Gao<sup>1</sup>, Yang (Michael) Yang<sup>1</sup>, Huanping Zhou<sup>1,2</sup>, Letian Dou<sup>1,2</sup>, Gang Li<sup>1</sup> & Yang Yang<sup>1,2</sup><sup>1</sup>Department of Materials Science and Engineering, University of California, Los Angeles, Los Angeles, California 90095, USA,<sup>2</sup>California NanoSystems Institute, University of California, Los Angeles, Los Angeles, California 90095, USA.Received  
25 September 2013Accepted  
7 November 2013Published  
28 November 2013Correspondence and  
requests for materials  
should be addressed to  
Y.Y. (yangy@ucla.edu)\* These authors  
contributed equally to  
this work.

A two-dimensional conjugated small molecule (SMPV1) was designed and synthesized for high performance solution-processed organic solar cells. This study explores the photovoltaic properties of this molecule as a donor, with a fullerene derivative as an acceptor, using solution processing in single junction and double junction tandem solar cells. The single junction solar cells based on SMPV1 exhibited a certified power conversion efficiency of 8.02% under AM 1.5 G irradiation (100 mW cm<sup>-2</sup>). A homo-tandem solar cell based on SMPV1 was constructed with a novel interlayer (or tunnel junction) consisting of bilayer conjugated polyelectrolyte, demonstrating an unprecedented PCE of 10.1%. These results strongly suggest solution-processed small molecular materials are excellent candidates for organic solar cells.

Organic solar cells (OSCs) have attracted significant attention due to their potential for low cost, light-weight, flexible and environmentally friendly energy-converting devices<sup>1-3</sup>. To separate the strongly bound Frenkel excitons in organic films, the donor-acceptor concept was proposed<sup>4</sup>. So far, fullerene C<sub>60</sub> and C<sub>70</sub>, as well their derivatives, are most successful acceptors for OSCs. Much work has been done to rationalize the energy levels and bandgap of donor materials in order to maximize photovoltaic efficiency. Since organic photovoltaic materials exhibit non-continuous absorption bands, it is not sufficient to cover the solar spectrum effectively with single junction devices. It is well known that tandem structures composed of two or more stacked photoactive layers with complementary absorption spectra have been considered as a promising approach to further enhance device performance<sup>5-7</sup>. To date, double-junction tandem OSCs using wide and low bandgap polymers have achieved a power conversion efficiency (PCE) as high as 10.6%<sup>7</sup>. On the other hand, for most high performance single-junction bulk heterojunction (BHJ) devices, the overall absorption of the active layer is well below 80% due to small film thickness limited by inferior carrier mobilities. Increasing film thickness elevates both absorption and short circuit current, yet also decreases fill factor (FF) due to recombination (shunt) loss and bulk (serial) resistance. Thus the absorption of incident photons is insufficient in optimized OSCs<sup>8-10</sup>. In order to have both sufficient absorption and efficient charge extraction, we can split a thick film into two thin subunits, shortening the travel distance of charge carriers for final collection at the electrodes. This means the tandem device via stacking the same subcells is feasible to enhance light harvesting. We call this structure as homo-tandem, since it consists of two heterojunctions based on same photoactive materials. Though the ultimate efficiency of such architecture is still subject to the Shockley-Queisser limit, it is surely a realistic way to maximize the photovoltaic efficiency from a given material. Recently, efficient homo-tandem OSC has been achieved by using a low bandgap polymer<sup>9</sup>. In addition, small molecule organic semiconductors have attracted increasing interest for preparing OSCs due to the advantages of its well-defined structures, facile synthesis and purification, and generally high V<sub>OC</sub><sup>11-14</sup>. Vacuum-deposited small molecule OSCs developed very fast and PCEs of up to 12% have been achieved using tandem structures<sup>15-18</sup>. On the other hand, devices fabricated via solution processing can improve the efficiency of the process and greatly reduce fabrication costs. Enormous progress has been made in the past few years to improve the PCE of the solution-processed devices from lower than 2% (before 2008) to higher than 7%, with a recent best PCE of 9.02%, making solution processed small molecule OSCs a very fast growing field<sup>11-14,19-21</sup>. However, small molecule based OSCs still require better material design and device engineering. Hence, it remains a challenge to develop high performance photovoltaic small molecules to fulfill the demands of the single junction and tandem OSCs with larger than 10% efficiency for practical applications.



To date, most photovoltaic polymers and small molecules have linear conjugated structures. It is well known that the extension of conjugation is one effective way to intensify and broaden the absorption spectra of conjugated polymers. In the past few years, two-dimensional (2-D) conjugated polymers with conjugated side chains have been developed to extend solar spectral coverage and enhance charge transport to improve device performance<sup>22–27</sup>. Recently, the alkylthienyl-substituted benzo[1,2-b:4,5-b']dithiophene (BDT-T) unit has emerged as an attractive 2-D conjugated building block for conjugated polymers<sup>23–25,27–29</sup>. Due to twisting of the thienyl plane with the BDT plane, this 2-D conjugated BDT-T unit using an alkylthienyl group is a weaker electron donor unit in comparison with the BDT unit with an alkoxy group for use in photovoltaic polymers, thus giving rise to a lower HOMO (highest occupied molecular orbital) level<sup>25,28</sup>. A deep HOMO level is desirable for obtaining high open-circuit voltage ( $V_{OC}$ ) since maximum value of the  $V_{OC}$  is determined by the energy difference between the HOMO level of the donor and LUMO (lowest unoccupied molecular orbital) level of the acceptor<sup>30</sup>. Thus solution-processed 2-D small molecules, though few, are known as good candidates for OSCs<sup>31,32</sup>, since the introduction of the 2D-conjugated structure in conjugated polymers has proven to be helpful in improving photovoltaic performance (PCE > 7%)<sup>24,29</sup>.

For conjugated molecules with acceptor-donor-acceptor (A-D-A) structure, many promising end-group acceptors have been reported; these include dicyanovinyl<sup>33,34</sup>, alkyl cyanoacetate<sup>35–38</sup> and 3-ethylrodanine<sup>39,40</sup>. Recently, Chen et al. reported an A-D-A small molecule comprised of a 3-ethylrodanine end-group, yielding a certified PCE of 7.6%<sup>41</sup>. In this work, we designed and synthesized a conjugated small molecule with a 2-D structure, SMPV1 (Fig. 1a), by introducing

BDT-T as the core unit and 3-octylrodanine as the electron-withdrawing end-group for use in solution-processed small molecule OSCs. We incorporated 3-octylrodanine end-cap units with long linear alkyl chains as promising electron-withdrawing units, which also work to improve solubility and film quality. Here, we report on the high performance single junction and double junction OSCs based on this 2-D conjugated small molecule. Furthermore, we developed a solution-processed bilayer structure of the conjugated polyelectrolyte (CPE), combined with PEDOT:PSS as interconnection layer (ICL) for the double junction homo-tandem device to further explore the utmost photovoltaic performance of this material. In the tandem cell, the overall thickness of the photoactive layer is almost doubled, reaching a PCE as high as 10.1%. The new ICL presented here offers a universal choice for tandem devices.

## Results

**Small molecule synthesis and characterization.** The chemical structure of SMPV1 is shown in Fig. 1a. The synthetic procedures and characterization data are given in the Supplementary Information. SMPV1 exhibits excellent solubility in organic solvents—such as  $\text{CHCl}_3$ , toluene and chlorobenzene—and shows a rather good thermal stability up to 402°C under argon, with a melting point at 185°C (Supplementary, Fig. S1). The absorption spectra of the SMPV1 in  $\text{CHCl}_3$  solution and in solid film are shown in Fig. 1c. SMPV1 exhibits absorption maxima at 508 nm in  $\text{CHCl}_3$  and the absorption onset at ~607 nm. Film absorption was red-shifted, having maxima at 584 nm and a shoulder peak at 627 nm. The peak absorption coefficient reaches  $4.8 \times 10^4 \text{ cm}^{-1}$ . The broadened absorption band was observed because of intermolecular  $\pi$ - $\pi$  packing interactions. Such an ordered packing of small molecule chains is

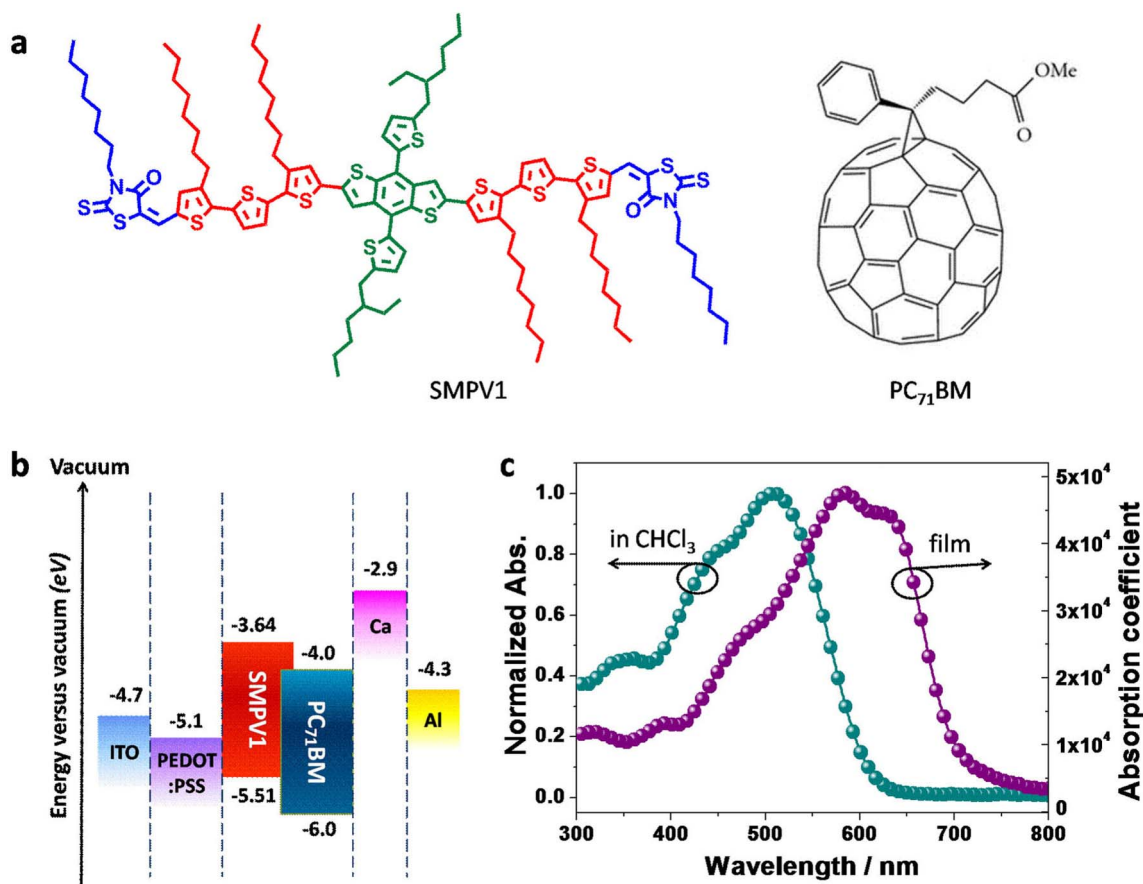


**Figure 1** | Molecular structure, energy levels and absorption spectra. (a), Molecular structure of SMPV1 and PC<sub>71</sub>BM. (b), Energy level of SMPV1 based single junction device. (c), Absorption spectra of SMPV1 in chloroform ( $\text{CHCl}_3$ ) and in solid film.

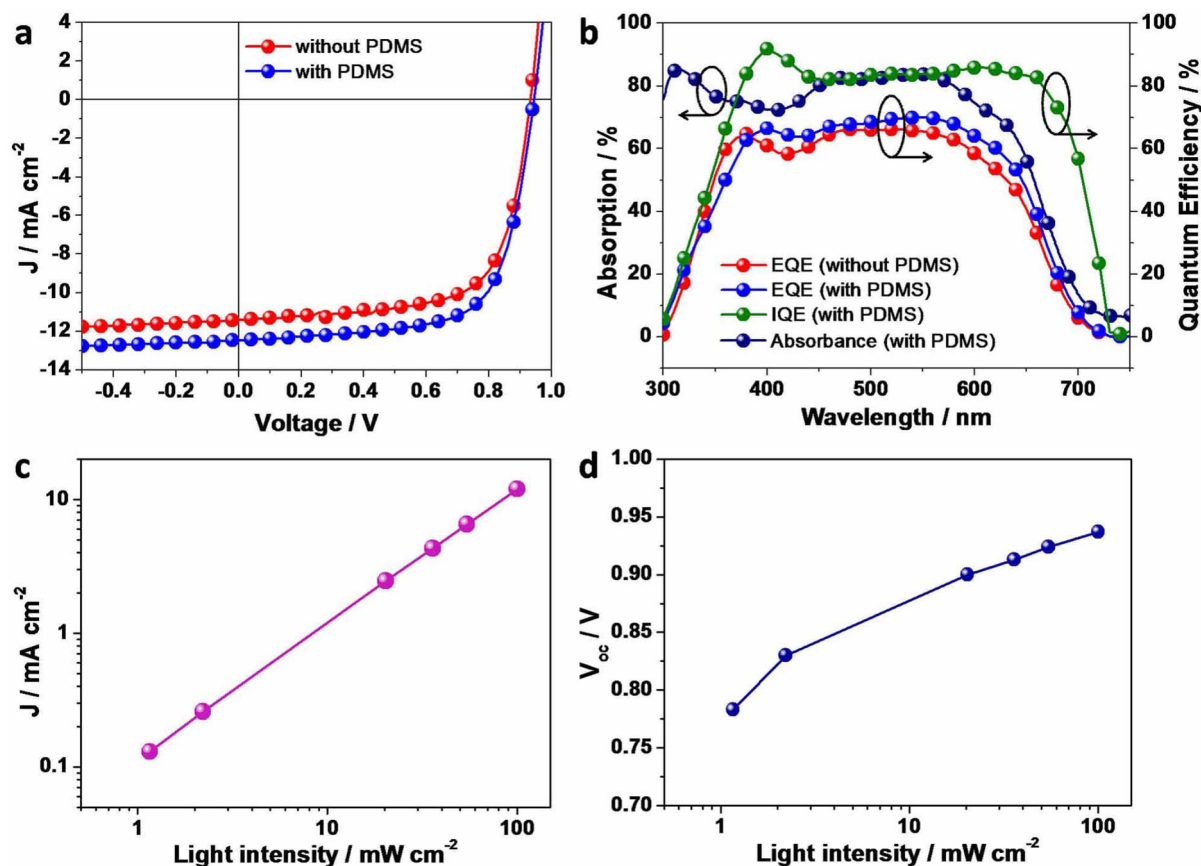


**Figure 2** | Device performance of single junction solar cells, and performance parameters of optimized device with PDMS (0.5 mg ml<sup>-1</sup>) as additive under varied light intensity (from 1.2 to 100 mW cm<sup>-2</sup>). (a), Current density versus voltage ( $J$ - $V$ ) curves under AM 1.5 G irradiation at 100 mW cm<sup>-2</sup>. (b), Absorption spectra, EQE and IQE. (c),  $J_{SC}$  as a function of light intensity in a double-logarithmic scale for devices using PDMS as additive. (d),  $V_{OC}$  as a function of light intensity in a semi-logarithmic scale for devices using PDMS as additive.

beneficial for carrier mobility as discussed below. The absorption onset of the SMPV1 film is located at  $\sim 699$  nm, corresponding to an optical bandgap of 1.77 eV. As shown in Fig. 1c, the SMPV1 shows strong absorption from 500 to 700 nm. To cover the short wavelength region, [6,6]-phenyl-C<sub>71</sub>-butyric acid methyl ester (PC<sub>71</sub>BM) was used as the acceptor for the BHJ OSCs. Cyclic voltammetry (Supplementary, Fig. S3) was recorded from thin film of SMPV1 drop-casted from chloroform solution. The measured HOMO and LUMO levels are  $-5.5$  and  $-3.6$  eV, respectively<sup>23</sup>. The electrochemical bandgap of SMPV1 is 1.9 eV, in agreement with its optical bandgap. The low lying HOMO level is favorable to generate high  $V_{OC}$  in BHJ OSCs<sup>30</sup>. The LUMO difference between SMPV1 ( $-3.6$  eV) and PC<sub>71</sub>BM ( $-4.0$  eV) is 0.4 eV, which shall be enough for exciton dissociation<sup>2</sup>.

**Single junction solar cells.** Single junction OSC devices are important building blocks for tandem architecture. Here we first tested SMPV1 in a device structure of ITO/PEDOT:PSS/SMPV1:PC<sub>71</sub>BM/Ca/Al. Current density-voltage ( $J$ - $V$ ) curves are shown in Fig. 2a and the

parameters listed in Table 1. With the optimized weight ratio of 1 : 0.8 for SMPV1:PC<sub>71</sub>BM, a PCE of 7.2% was obtained, with a  $J_{SC}$  of 11.4 mA cm<sup>-2</sup>, a  $V_{OC}$  of 0.93 V, and an FF of 68%. By adding 0.5 mg mL<sup>-1</sup> PDMS<sup>40,42</sup> in the blend solution, the PCE was further improved to 8.1%, with a  $V_{OC}$  of 0.94 V, a  $J_{SC}$  of 12.5 mA cm<sup>-2</sup>, and a notable FF of 69%. The encapsulated device was sent to the Newport Corporation for certification. A certified efficiency of 8.02% was obtained, as shown in Fig. S14 (Supplementary information).

The external quantum efficiency (EQE) and the absorption (extracted from reflection spectrum ( $R\%$ ) by  $100-R$ ) of the optimized devices are illustrated in Fig. 2b. The pristine SMPV1/PC<sub>71</sub>BM (w/w, 1 : 0.8) BHJ devices exhibit a broad and high photoresponse from 300 to 700 nm, with EQE peak reaching 64.1% at 550 nm. With PDMS as a processing additive, the EQE was further enhanced in the entire photoresponse range, and reached a maximum of 70% at 550 nm, leading to 9% enhancement in  $J_{SC}$ . The internal quantum efficiency (IQE) of the optimized single junction device was then calculated using EQE and absorption data. The result is shown in Fig. 2b and Fig. S4 (Supplementary). In almost the whole photon-to-current

**Table 1** | Solar cell parameters of single junction and double junction tandem devices prepared from SMPV1/PC<sub>71</sub>BM

Active layer	$V_{OC}$ (V)	$J_{SC}$ (mA cm <sup>-2</sup> )	PCE (%)	FF (%)
<b>Single junction</b>	0.93	11.4	7.2	68
<b>Single junction<sup>a</sup></b>	0.94	12.5	8.1	69
<b>Single junction<sup>a</sup> (Newport Certified)</b>	0.937	12.17	8.02	70.4
<b>Tandem<sup>a</sup></b>	1.82	7.7	10.1	72

<sup>a</sup>PDMS (0.5 mg ml<sup>-1</sup>) was added to the active materials solution.





range (380 to 680 nm), the averaged IQE of the device with PDMS additive was over 80%, which is higher than that of the device without PDMS additive. This clearly indicates that the PDMS additive plays a positive role in free carrier generation in the BHJ films, which may result from more effective donor/acceptor interface due to the decreased domain size as discussed in the morphology section below. However, we noticed that the photocurrent from single junction OSC was limited by the optical absorption. As shown in Fig. 2b, the average absorption of the active layer in reflection mode is merely 80%. Therefore, we expect higher photocurrent and PCE, if we can enhance the visible absorption and maintain the highly efficient charge transport and collection simultaneously. We will show later that the absorption issue can be addressed by using tandem architecture.

Here we go further to explore the carrier recombination in the device by measuring light intensity dependence of J-V characteristics under illumination of solar simulator with a set of neutral density filters. Fig. 2c shows a linear relation of photocurrent on light intensity in a double logarithmic scale with a slope of 1.01<sup>43</sup>. Thus, bimolecular recombination is a rather minor loss. Fig. 2d gives  $V_{OC}$  as a function of the logarithm of light intensity. We can see that  $V_{OC}$  increases monotonically with light intensity. The experimental data is fitted with a linear function with a slope of  $\sim 2.0$  kT/q from 0.1 sun to 1 sun, and  $\sim 3.0$  kT/q below 0.1 sun, suggesting that trap-assisted recombination only play a role at low light intensity, where  $k$  is Boltzmann's constant,  $T$  is temperature, and  $q$  is elementary charge<sup>44</sup>. This partially explains why our single junction OSCs work efficiently.

Bearing in mind that the high FF indicates very low recombination loss and serial resistance in the BHJs, it is worth further investigation on the structural ordering of SMPV1 molecules, since it is closely related to charge transporting properties. The crystalline structures of BHJ films in optimized device conditions were characterized using X-ray diffraction (XRD) as shown in Fig. 3. The detailed  $d$ -spacing values are summarized in Table S1 (Supplementary). SMPV1 molecules show high crystallinity, which is tentatively attributed to the strong self-assembly into an ordered lamellar structure. As shown in Fig. 3, the  $\pi$ -conjugated molecules exhibited a strong (100) reflection peak at  $2\theta = 4.18^\circ$ , corresponding to a  $d_{100}$ -spacing value of 21.1 Å. The XRD of SMPV1/PC<sub>71</sub>BM (1 : 0.8, w : w) blend film shows a small, but sharp (100) reflection peak at  $2\theta = 4.22^\circ$ , corresponding to a  $d_{100}$ -spacing of 20.9 Å, which is similar with that of the pristine SMPV1 film. It indicates the lamellar structures of the conjugated molecules sustain even when PC<sub>71</sub>BM is added. In Fig. 3, weak but sharp (100) reflection peaks are observed from the blend film using PDMS as an additive, suggesting the lamellar structure of donor materials are still maintained, which benefits the charge transport.

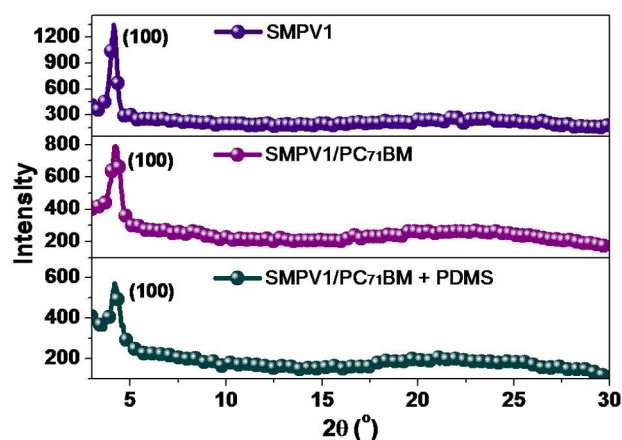


**Figure 3** | X-ray diffraction (XRD) analyse. XRD patterns of SMPV1, SMPV1/PC<sub>71</sub>BM (1 : 0.8) films with and without PDMS additive spin-coated from CHCl<sub>3</sub> on glass substrates.

Thus we look into the charge transport in the optimized active layer. A structure of ITO/PEDOT:PSS/SMPV1:PC<sub>71</sub>BM/Au was built up as hole-only devices, and ITO/Al/SMPV1:PC<sub>71</sub>BM/Ca/Al as electron-only devices. The current density–voltage (J-V) characteristics of hole-only and electron-only devices are shown in Fig. S5 (Supplementary). By fitting the J-V curves to the space charge limited current (SCLC) model, carrier mobilities can be derived. Relatively high carrier mobilities on the order of  $10^{-4}$  cm<sup>2</sup> v<sup>-1</sup> s<sup>-1</sup> were observed in both BHJs with and without PDMS. As a matter of fact, SMPV1 based photovoltaic devices have high FF and low serial resistance, no matter PDMS is added or not. The only difference is photocurrent enhancement upon adding PDMS. This led us to view this issue in a different angle. For the device without PDMS additive, the hole mobility was  $3.4 \times 10^{-4}$  cm<sup>2</sup> v<sup>-1</sup> s<sup>-1</sup>, and the electron mobility was  $8.1 \times 10^{-4}$  cm<sup>2</sup> v<sup>-1</sup> s<sup>-1</sup>. The active layer with PDMS as additive exhibits more balanced hole and electron mobility of  $3.3 \times 10^{-4}$  and  $6.3 \times 10^{-4}$  cm<sup>2</sup> V<sup>-1</sup> s<sup>-1</sup>, respectively, which is consistent with higher FF and  $J_{SC}$ , thus concluding the better device performs with use of PDMS additive.

**Morphology.** In order to understand the effects of PDMS on photovoltaic performance, we then carried out a morphology study of the active layer. It is well-known that a nanoscale phase separation and bicontinuous interpenetrating network in the active layer is necessary to efficiently separate the exciton and form percolating channels for the transport of both holes and electrons. The surface morphologies of the SMPV1/PC<sub>71</sub>BM (1 : 0.8, w : w) films with and without PDMS were characterized using tapping-mode atomic force microscopy (AFM). Surface topography and phase images were taken for both films as shown in Fig. 4. Both blend films are smooth and uniform, which is critical to minimize electrical leakage. The root-means-square (rms) roughness of blend film with PDMS is 0.51 nm, similar to that of the pristine one, 0.77 nm. In comparison with the pristine-blend film, the height images of the films with PDMS shows nano-fibrillar features. Phase images of the two films show different features, as shown in Fig. 4. Because phase contrast is related to the difference in adhesive and mechanical properties of individual materials, this clearly indicates that the dark and bright parts can be differentiated as different components. Nanoscale phase separation and bicontinuous interpenetrating network can be clearly observed. It is noted that the irregular-shape domains have an average size of 20–30 nm in blend film with PDMS, which is beneficial for charge generation and transport, whereas the sample without PDMS has larger domain size about 50 nm. Large domain sizes can be regarded as a challenging issue in OSCs, since the exciton diffusion length is usually small. And in this case, the excitons in the film without PDMS may not be able to reach the donor/acceptor interface, and to subsequently dissociate into free carriers.

AFM only allows us to see the film surface morphology. To obtain further insight in active layer morphology in 3-dimension, we recorded high resolution transmission electron microscopy (HRTEM) images of the active layers without and with additive, and the results are shown in Fig. 4c and Fig. 4f. The bright and dark regions can be attributed to SMPV1-rich domains and PC<sub>71</sub>BM-rich domains, respectively, because pure SMPV1 domains should appear brighter in TEM images due to its lower electron density than that of PC<sub>71</sub>BM<sup>8</sup>. It is found that SMPV1:PC<sub>71</sub>BM-blend film with PDMS as an additive has promoted fine features of phase separation and has induced the nanofibril formation, thus plausibly interpenetrating networks (Fig. 4f) form, whereas the pristine-blend film shows relatively large domains (Fig. 4c), which is consistent with the AFM. Therefore we conclude that PDMS additive induces finer phase separation in the BHJs, and enhances charge generation.

**CPE ICL for double junction tandem device.** As mentioned above, the optimal thickness of the BHJs limits overall absorption. To

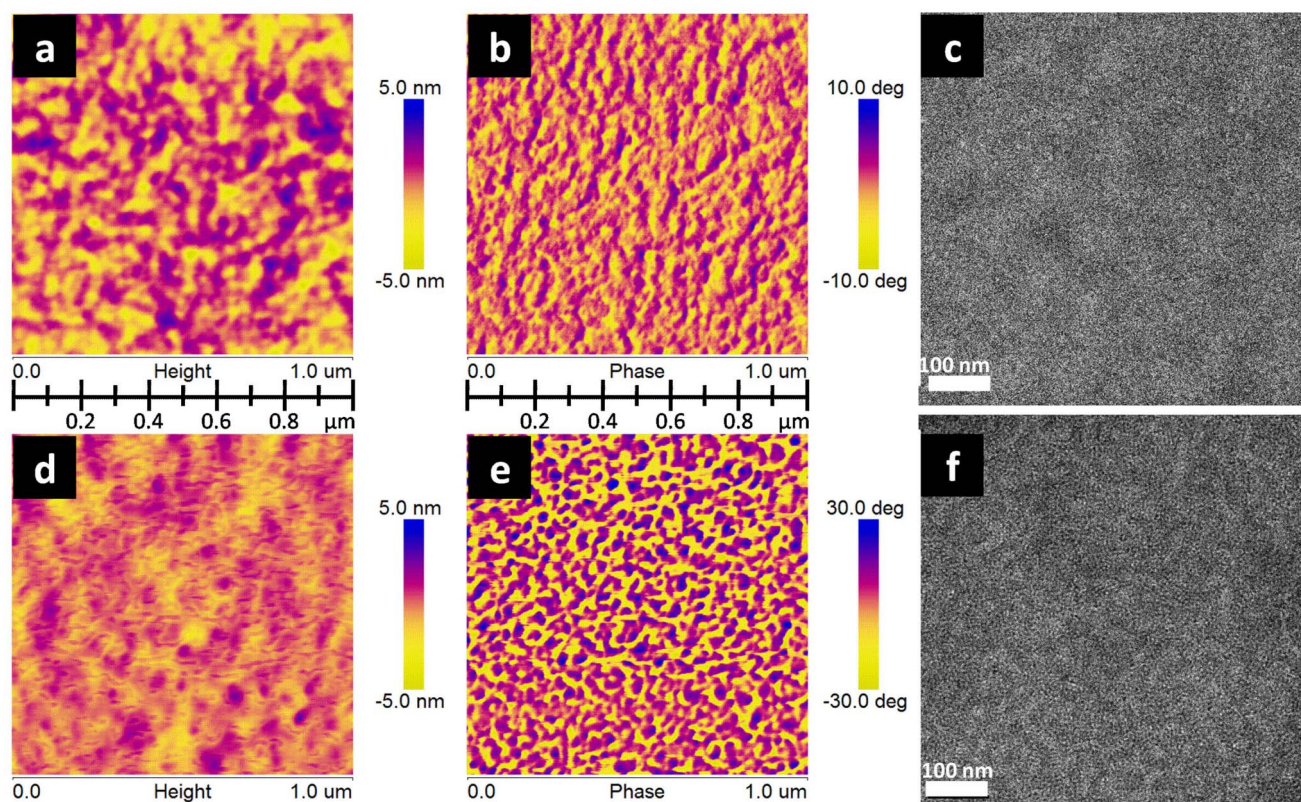


**Figure 4** | Tapping-mode AFM and HRTEM of BHJ films without and with PDMS ( $0.5 \text{ mg ml}^{-1}$ ) as additive. a,b,c, height (a) and phase (b) images ( $1 \times 1 \mu\text{m}$ ), and HRTEM (c) images of the film without PDMS additive. (d), (e), (f), height (d) and phase (e) images ( $1 \times 1 \mu\text{m}$ ), and HRTEM (f) images of the film with PDMS ( $0.5 \text{ mg ml}^{-1}$ ) as additive.

circumvent this challenge, we designed a solution processed, thermal annealing-free ICL for tandem solar cells based on SMPV1:PC<sub>71</sub>BM BHJs. Recently, Wu et al. have demonstrated another efficient electron transporting layer material using conjugated polyelectrolyte (CPE) on top of the polymer active layer<sup>45</sup>. The formation of a surface dipole at interface between the photoactive layer and metal electrode can suppress the interfacial recombination, and thus improve the device performance. Due to superior electrical properties of CPE as cathode buffer layer in OSCs, it is highly desirable to incorporate it into tandem architectures, in combination with an anode buffer layer. However, the problem with monolayer films is that they were not capable of being modified to achieve desired surface characteristics because of its small thickness<sup>45</sup>. Thus, the demonstration of interconnecting layers composed of CPE in the tandem solar cell is rarely found.

We developed a multilayered film having a well-defined molecular organization in a smooth geometrical arrangement as interconnecting layer (ICL). Tandem solar cells comprising two identical photoactive layers as subcells based on SMPV1:PC<sub>71</sub>BM were then fabricated. The device structure is ITO/PEDOT:PSS/SMPV1:PC<sub>71</sub>BM/CPE1/CPE2/M-PEDOT:PSS/SMPV1:PC<sub>71</sub>BM/CPE3/Al, as shown in Fig. 6a. The chemical structure of CPE1, CPE2 and CPE3 are shown in Fig. 5. First, a CPE bilayer consisting of a polycation with its corresponding counterion and a polyanion with its corresponding counterion was deposited on the front subcell in sequence to form an efficient pathway for electron transport. The self-assembly of the CPE bilayer occurs due to opposite charges on each adjacent layer, and thus can improve its solvent resistivity by strong ionic bonding. It also creates an internal polarization field that can shift up vacuum levels and lower the electron injection barrier from the front subcell to the middle ICL, as shown in Fig. 6c<sup>46</sup>.

In Fig. 6d, the J-V curve of a tandem solar cell comprising of two identical photoactive layers as subcells is shown in comparison with

that of single junction solar cell. Given the best performance of single junction device is at 8.1% efficiency, the optimized tandem solar cell can achieve a PCE of 10.1%, corresponding to a 25% enhancement with a  $V_{OC}$  of 1.82 V, a  $J_{SC}$  of  $7.70 \text{ mA cm}^{-2}$ , and a very notable FF of 72%. The CPE based ICL can be considered as Ohmic contact with negligible resistance, resulting in high FF in the tandem cell. The origin of improvement comes from increased optical absorption (see Supplementary Fig. S7). We define the EQE of the tandem cell as the ratio of total converted carriers in the two subcells to the sum of incident photons, which can be calculated using IQE of single junction devices<sup>9</sup>. From Fig. 6e, the estimated EQE of tandem device increased dramatically by 30% as compared to that of single junction device. In another method, we measure the photoresponse of the tandem cell and multiply it by two to represent the total number of photons being converted to electrons, the estimated EQE of the tandem cell. Then, dividing this EQE by absorption of tandem cell under reflection mode, we obtain estimated IQE. As shown in Fig. 6f, the IQE of the tandem cell is similar to that of single junction device, which indicates that charge extraction is as efficient as it is in the single junction cell. Therefore a tandem structure can increase the overall optical absorption without sacrificing the IQE, owing to its excellent ICL, and thus can ensure almost complete utilization of all the photon energy in its absorption range.

## Discussion

The full solution processed, thermal annealing-free ICL we developed plays an important role in our small molecule based homo-tandem device. In order to obtain the correct polarization direction of the bilayer CPE films, the polycation with a positively charged amine functional group (CPE1) is placed near the photoactive layer while the polyanion with a negatively charged  $-\text{SO}_3^-$  functional group (CPE2) is applied as the outermost layer. As shown in Fig. 6b, the



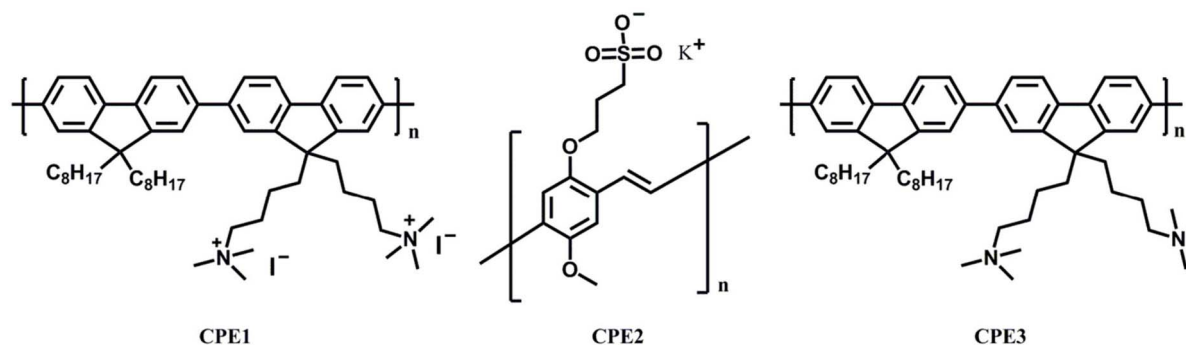


**Figure 5** | Chemical structure of CPE1, CPE2 and CPE3.

spontaneous orientation from the ionic group of CPE and its corresponding counterion leads to the formation of permanent dipoles between at the active layer of the front cell and M-PEDOT:PSS interface. After the completion of bilayer CPE structure, M-PEDOT:PSS containing both polyanion, PSS, and polycation, PEDOT, is applied as a hole transporting layer for the back subcell. Due to the positively charged functional group, PEDOT is likely to be “pinned” down in the bottom of film by ionic interaction with the already existing polyanion layer. At the same time, the PSS with low surface energy has a tendency to float to the top of the film leaving the outermost surface of ICL to have negatively charged surface which is beneficial to the hole injection from back subcell<sup>47</sup>. As a result, we performed a well-organized multilayer charge film to achieve a precise charge distribution and surface polarization, which optimizes the charge injection of front and back subcell and facilitates the charge recombination. The key features of CPE based ICL are thermal treatment-

free processing which is found to be crucial in maintaining the optimized morphology of small molecular tandem solar cell.

In conclusion, we have successfully demonstrated high-efficiency solution-processed single junction and double junction tandem OSCs based on a 2-D conjugated small molecule. Single junction device based on SMPV1/PC<sub>71</sub>BM exhibited a certified PCE of 8.02% under AM1.5G one-sun illumination, as measured by Newport Corporation. A simple solution-processed ICL based on bilayer CPE was developed to build up tandem solar cells using this 2-D small molecule as the photoactive material, exhibiting a high PCE of 10.1%. Our results show the great potential of the 2-D conjugated small molecule for high performance BHJ OSCs.

## Methods

Materials and methods, complete synthesis and characterization of SMPV1, TGA, DSC, cyclic voltammetry plots, XRD, additional ultraviolet visible absorption spectra,

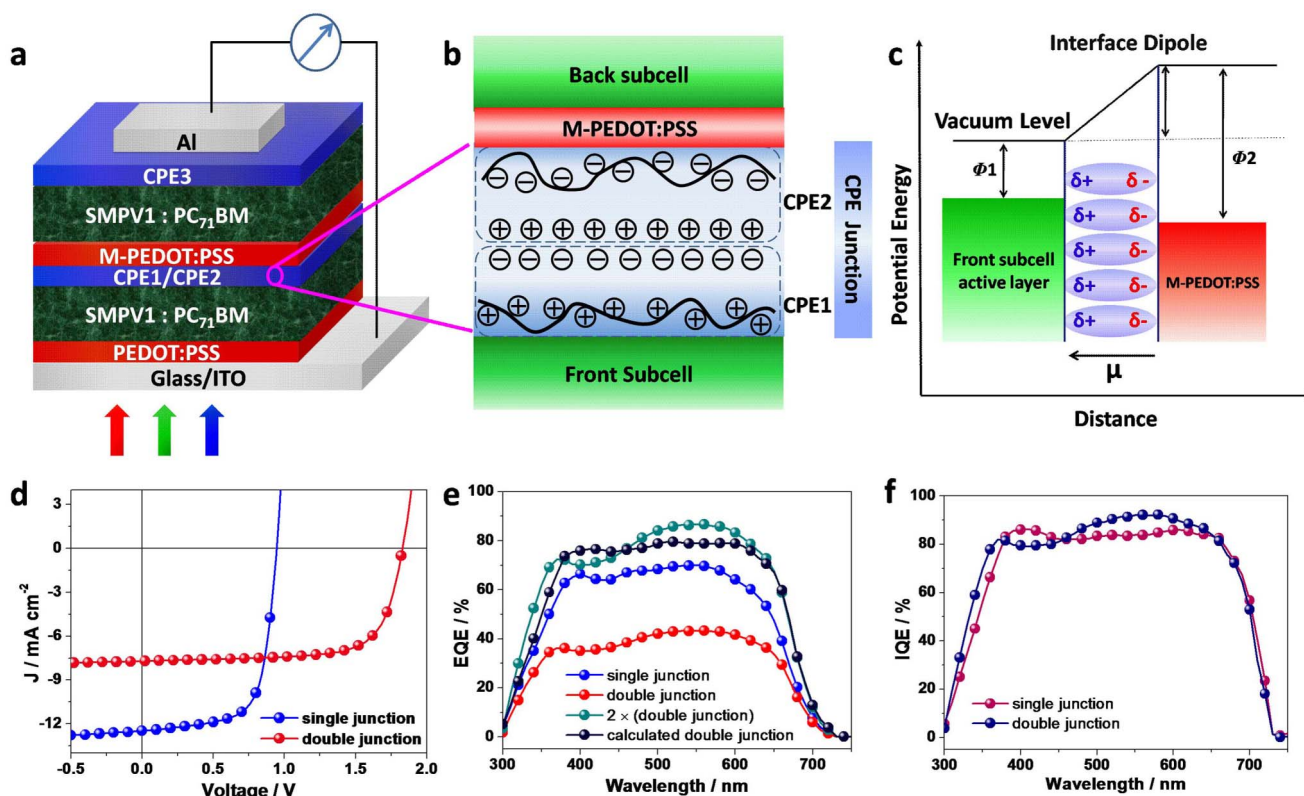


**Figure 6** | Homo-tandem solar cells. (a), Device structure. (b), Proposed scenario of self-assembly bilayer CPE. (c), Proposed schematic energy diagram of the origin of the work function change due to the presence of CPE between the front subcell and the back subcell. (d), J–V characteristics of the single junction and tandem solar cells. (e), EQE of the tandem solar cells, for comparison, EQE of single junction solar cells and calculated total EQE of the tandem solar cells based on total absorption and sub-cells IQE, and EQE of single junction device are included. (f), Calculated IQEs of the tandem solar cells based on the total absorption and EQE of the tandem solar cells, IQE of single junction device is included for comparison.



J-V curves, EQE spectra, and AFM characterization can be found in the Supplementary Information.

**Single junction device fabrication.** The pre-cleaned ITO substrates were first treated with UV-ozone for 20 min. A thin layer of PEDOT:PSS (Baytron P VP AI 4083, filtered at 0.2  $\mu\text{m}$ ) was spin-coated (4000 rpm, ca. 40 nm thick) onto an ITO surface. After being baked at 120°C for 15 minutes, the substrates were transferred into a nitrogen-filled glove box. Subsequently, the active layer was spin-coated from a different blend ratio (weight-to-weight, w:w) of a conjugated small molecule (14 mg mL<sup>-1</sup>) and PC<sub>71</sub>BM in chloroform solution on the ITO/PEDOT:PSS substrate. For the active layers fabricated with PDMS additive, PDMS with desired amounts was added in the donor/PC<sub>71</sub>BM blend solutions and stirred for 1 hour before spin-coating. The active layer thickness was measured as ~120 nm using a Dektak 150 profilometer. Finally, a 20 nm Ca layer and a 100 nm Al layer were deposited in sequence on the active layer through shadow masks via thermal evaporation under high vacuum (~2 × 10<sup>-6</sup> Torr). The effective area was 0.10 cm<sup>2</sup>. The certified single junction device was measured using a shadow mask with an area of 0.0411 cm<sup>2</sup>.

**Tandem device fabrication.** The device architecture of the tandem solar cell is shown in Fig. 6a. Photoactive layers were fabricated via same process as single junction cells. Then the CPE1 (0.02 wt% in methanol) and CPE2 (0.02 wt% in deionized water) were spin-coated on the active layer of the front cell in sequence. Both the thickness of CPE1 and CPE2 are about 5 nm<sup>45</sup>. Then modified PEDOT:PSS (M-PEDOT:PSS) were spin-coated on CPE2 surface. The details of M-PEDOT:PSS can be found in the literature, the only difference is that PEDOT:PSS (Baytron P VP AI 4083) was used here to avoid parasitic current<sup>48</sup>. The active layer was then spin-coated. The active layer thickness of front cell and back cell are ~80 nm and ~100 nm, respectively. After that, a thin layer of CPE3 (0.02 wt% in methanol) was spin coated. The device fabrication was completed by thermal evaporation of 100 nm Al as cathode under high vacuum (~2 × 10<sup>-6</sup> Torr).

**Device characterization.** The current density-voltage (J-V) characteristics of photovoltaic devices were obtained by a Keithley 2400 source-measure unit. The photocurrent was measured under AM 1.5 G illumination at 100 mW cm<sup>-2</sup> under a Newport Thermal Oriol 91192 1000 W solar simulator. The light intensity was determined by a Si photodiode as a reference cell. The reflection of the device has been measured to evaluate the total absorption of the device, and the absolute absorption of the devices was calculated by (100-R)%. The reflection was carried out using Varian Cary 50 UV-Visible Spectrophotometer with a reflection accessory.

1. Su, Y. W., Lan, S. C. & Wei, K. H. Organic photovoltaics. *Mater Today* **15**, 554–562 (2012).
2. Li, G., Zhu, R. & Yang, Y. Polymer solar cells. *Nat. Photonics* **6**, 153–161 (2012).
3. Kumar, P. & Chand, S. Recent progress and future aspects of organic solar cells. *Prog. Photovoltaics* **20**, 377–415 (2012).
4. Tang, C. W. 2-Layer Organic Photovoltaic Cell. *Appl. Phys. Lett.* **48**, 183–185 (1986).
5. Kim, J. Y. *et al.* Efficient tandem polymer solar cells fabricated by all-solution processing. *Science* **317**, 222–225 (2007).
6. Li, W. W., Furlan, A., Hendriks, K. H., Wienk, M. M. & Janssen, R. A. J. Efficient Tandem and Triple-Junction Polymer Solar Cells. *J. Am. Chem. Soc.* **135**, 5529–5532 (2013).
7. You, J. B. *et al.* A polymer tandem solar cell with 10.6% power conversion efficiency. *Nat. Commun.* **4**, 1446 (2013).
8. Park, S. H. *et al.* Bulk heterojunction solar cells with internal quantum efficiency approaching 100%. *Nat. Photonics* **3**, 297–U295 (2009).
9. You, J. B. *et al.* 10.2% Power Conversion Efficiency Polymer Tandem Solar Cells Consisting of Two Identical Sub-Cells. *Adv. Mater.* **25**, 3973–3978 (2013).
10. Chen, C. C. *et al.* High-performance semi-transparent polymer solar cells possessing tandem structures. *Energ. Environ. Sci.* **6**, 2714–2720 (2013).
11. Lin, Y. Z., Li, Y. F. & Zhan, X. W. Small molecule semiconductors for high-efficiency organic photovoltaics. *Chem. Soc. Rev.* **41**, 4245–4272 (2012).
12. Mishra, A. & Bauerle, P. Small Molecule Organic Semiconductors on the Move: Promises for Future Solar Energy Technology. *Angew. Chem. Int. Edit.* **51**, 2020–2067 (2012).
13. Walker, B., Kim, C. & Nguyen, T. Q. Small Molecule Solution-Processed Bulk Heterojunction Solar Cells. *Chem. Mater.* **23**, 470–482 (2011).
14. Wurthner, F. & Meerholz, K. Systems Chemistry Approach in Organic Photovoltaics. *Chem-Eur. J.* **16**, 9366–9373 (2010).
15. Riede, M. *et al.* Efficient Organic Tandem Solar Cells based on Small Molecules. *Adv. Funct. Mater.* **21**, 3019–3028 (2011).
16. Fitzner, R. *et al.* Correlation of pi-Conjugated Oligomer Structure with Film Morphology and Organic Solar Cell Performance. *J. Am. Chem. Soc.* **134**, 11064–11067 (2012).
17. Chen, Y. H. *et al.* Vacuum-Deposited Small-Molecule Organic Solar Cells with High Power Conversion Efficiencies by Judicious Molecular Design and Device Optimization. *J. Am. Chem. Soc.* **134**, 13616–13623 (2012).
18. Heliatek consolidates its technology leadership by establishing a new world record for organic solar technology with a cell efficiency of 12%. [http://www.heliatek.com/wp-content/uploads/2013/01/130116\\_PR\\_Heliatek\\_achieves\\_record\\_cell\\_efficiency\\_for\\_OPV.pdf](http://www.heliatek.com/wp-content/uploads/2013/01/130116_PR_Heliatek_achieves_record_cell_efficiency_for_OPV.pdf). (October 2013 accessed).

19. Roncali, J. Molecular Bulk Heterojunctions: An Emerging Approach to Organic Solar Cells. *Accounts. Chem. Res.* **42**, 1719–1730 (2009).
20. Wei, G. D. *et al.* Efficient, Ordered Bulk Heterojunction Nanocrystalline Solar Cells by Annealing of Ultrathin Squaraine Thin Films. *Nano. Lett.* **10**, 3555–3559 (2010).
21. Gupta, V. *et al.* Barium: An Efficient Cathode Layer for Bulk-heterojunction Solar Cells. *Sci. Rep.* **3**, 1965 (2013).
22. Chen, C. C. *et al.* Visibly Transparent Polymer Solar Cells Produced by Solution Processing. *ACS. Nano.* **6**, 7185–7190 (2012).
23. Dou, L. T. *et al.* Systematic Investigation of Benzodithiophene- and Diketopyrrolopyrrole-Based Low-Bandgap Polymers Designed for Single Junction and Tandem Polymer Solar Cells. *J. Am. Chem. Soc.* **134**, 10071–10079 (2012).
24. Huang, Y. *et al.* Improving the Ordering and Photovoltaic Properties by Extending pi-Conjugated Area of Electron-Donating Units in Polymers with D-A Structure. *Adv. Mater.* **24**, 3383–3389 (2012).
25. Huo, L. J., Hou, J. H., Zhang, S. Q., Chen, H. Y. & Yang, Y. A Polybenzo[1,2-b:4,5-b']dithiophene Derivative with Deep HOMO Level and Its Application in High-Performance Polymer Solar Cells. *Angew. Chem. Int. Edit.* **49**, 1500–1503 (2010).
26. Li, Y. F. Molecular Design of Photovoltaic Materials for Polymer Solar Cells: Toward Suitable Electronic Energy Levels and Broad Absorption. *Accounts. Chem. Res.* **45**, 723–733 (2012).
27. Wang, M. *et al.* Donor Acceptor Conjugated Polymer Based on Naphtho[1,2-c:5,6-c']bis[1,2,5]thiadiazole for High-Performance Polymer Solar Cells. *J. Am. Chem. Soc.* **133**, 9638–9641 (2011).
28. Dou, L. T. *et al.* Tandem polymer solar cells featuring a spectrally matched low-bandgap polymer. *Nat. Photonics* **6**, 180–185 (2012).
29. Huo, L. J. *et al.* Replacing Alkoxy Groups with Alkylthienyl Groups: A Feasible Approach To Improve the Properties of Photovoltaic Polymers. *Angew. Chem. Int. Edit.* **50**, 9697–9702 (2011).
30. Scharber, M. C. *et al.* Design rules for donors in bulk-heterojunction solar cells - Towards 10% energy-conversion efficiency. *Adv. Mater.* **18**, 789–794 (2006).
31. Cui, C. H. *et al.* A new two-dimensional oligothiophene end-capped with alkyl cyanoacetate groups for highly efficient solution-processed organic solar cells. *Chem. Commun.* **49**, 4409–4411 (2013).
32. Huang, J. H. *et al.* Solution-Processed DPP-Based Small Molecule that Gives High Photovoltaic Efficiency with Judicious Device Optimization. *ACS. Appl. Mater. Inter.* **5**, 2033–2039 (2013).
33. Liu, Y. S. *et al.* Efficient solution processed bulk-heterojunction solar cells based a donor-acceptor oligothiophene. *J. Mater. Chem.* **20**, 2464–2468 (2010).
34. Schulze, K. *et al.* Efficient vacuum-deposited organic solar cells based on a new low-bandgap oligothiophene and fullerene C-60. *Adv. Mater.* **18**, 2872–2875 (2006).
35. Liu, Y. S. *et al.* High-Performance Solar Cells using a Solution-Processed Small Molecule Containing Benzodithiophene Unit. *Adv. Mater.* **23**, 5387–5391 (2011).
36. Liu, Y. S. *et al.* Spin-Coated Small Molecules for High Performance Solar Cells. *Adv. Energy. Mater.* **1**, 771–775 (2011).
37. Zhou, J. Y. *et al.* A Planar Small Molecule with Dithienosilole Core for High Efficiency Solution-Processed Organic Photovoltaic Cells. *Chem. Mater.* **23**, 4666–4668 (2011).
38. Liu, Y. S. *et al.* Solution-Processed Small Molecules Using Different Electron Linkers for High-Performance Solar Cells. *Adv. Mater.* **25**, 4657–4662 (2013).
39. Li, Z. *et al.* Solution Processable Rhodanine-Based Small Molecule Organic Photovoltaic Cells with a Power Conversion Efficiency of 6.1%. *Adv. Energy. Mater.* **2**, 74–77 (2012).
40. Zhou, J. Y. *et al.* Small Molecules Based on Benzo[1,2-b:4,5-b']dithiophene Unit for High-Performance Solution-Processed Organic Solar Cells. *J. Am. Chem. Soc.* **134**, 16345–16351 (2012).
41. Zhou, J. Y. *et al.* Solution-Processed and High-Performance Organic Solar Cells Using Small Molecules with a Benzodithiophene Unit. *J. Am. Chem. Soc.* **135**, 8484–8487 (2013).
42. Graham, K. R. *et al.* Polydimethylsiloxane as a Macromolecular Additive for Enhanced Performance of Molecular Bulk Heterojunction Organic Solar Cells. *ACS Appl. Mater. Inter.* **3**, 1210–1215 (2011).
43. Riedel, I. & Dyakonov, V. Influence of electronic transport properties of polymer-fullerene blends on the performance of bulk heterojunction photovoltaic devices. *Phys. Status. Solidi. A.* **201**, 1332–1341 (2004).
44. Mandoc, M. M., Kooistra, F. B., Hummelen, J. C., de Boer, B. & Blom, P. W. M. Effect of traps on the performance of bulk heterojunction organic solar cells. *Appl. Phys. Lett.* **91**, 263505 (2007).
45. He, Z. C. *et al.* Enhanced power-conversion efficiency in polymer solar cells using an inverted device structure. *Nat. Photonics* **6**, 591–595 (2012).
46. Khodabakhsh, S. *et al.* Using self-assembling dipole molecules to improve hole injection in conjugated polymers. *Adv. Funct. Mater.* **14**, 1205–1210 (2004).
47. Lee, T. W., Chung, Y., Kwon, O. & Park, J. J. Self-organized gradient hole injection to improve the performance of polymer electroluminescent devices. *Adv. Funct. Mater.* **17**, 390–396 (2007).
48. Yang, J. *et al.* A Robust Inter-Connecting Layer for Achieving High Performance Tandem Polymer Solar Cells. *Adv. Mater.* **23**, 3465–3470 (2011).

## Acknowledgments

The authors gratefully acknowledge the financial support from the Office of Naval Research (Grant No. N000141110250), National Science Foundation (Grant No. DMR-1335645),



and the Enli Tech (in Taiwan) for donating the EQE measurement system to UCLA. Further gratitude stems to Dr. W.B. Yang for his assistance with the TGA and DSC measurements, as well as to Dr. J.B. You and Dr. Q. Chen for helpful discussion. Y. Yang and G. Li also like to thank Prof. Y. Cao and H.B. Wu of the South China University of Technology for the discussion of polyelectrolyte. The authors in particular thank M. O'Donnell at Newport Corporation for his support in certifying the performance of our devices. The authors would lastly like to thank and acknowledge the use of the Nano and Pico Characterization Lab at the California NanoSystems Institute for AFM and TEM analysis.

### Author contributions

Y.L. and C.C. contributed equally to this work. Y.L., C.C. and Y.Y. developed the ideas. Y.L. designed SMPV1 and performed material synthesis and characterization. Y.L. carried out the fabrication, characterization of single junction devices, data collection and analysis. C.C. carried out the fabrication, characterization of tandem devices, data collection and analysis. C.C. and J.G. conceived the idea of a double CPE interlayer. Z.H. guided device testing at UCLA and coordinated certification. J.G. fabricated the single junction cell with a CPE interlayer. Y.M.Y. carried out light intensity measurements and partly participated in single

junction device testing. H.Z. carried out TEM measurements. J.G. partly supported with the TEM measurements. Y.L., C.C., Z.H. and Y.Y. prepared the manuscript. L.D. and G.L. contributed to the manuscript preparation. All authors discussed the results and commented on the manuscript. Y.Y. conceptualized, planned and supervised the project.

### Additional information

**Supplementary information** accompanies this paper at <http://www.nature.com/scientificreports>

**Competing financial interests:** The authors declare no competing financial interests.

**How to cite this article:** Liu, Y.S. *et al.* Solution-processed small-molecule solar cells: breaking the 10% power conversion efficiency. *Sci. Rep.* 3, 3356; DOI:10.1038/srep03356 (2013).



This work is licensed under a Creative Commons Attribution-NonCommercial-NoDerivs 3.0 Unported license. To view a copy of this license, visit <http://creativecommons.org/licenses/by-nc-nd/3.0>